ELSEVIER

Tectonophysics 333 (2001) 323–345

TECTONOPHYSICS

www.elsevier.com/locate/tecto

Structural, geodetic and seismological evidence for tectonic escape in SW Taiwan

O. Lacombe*, F. Mouthereau, J. Angelier, B. Deffontaines

Tectonique ESA 7072, Université P. et M. Curie, T26-25, E1, Boîte 129, 4 pl. Jussieu, 75252 Paris Cedex 05, France

Abstract

Recent structural, geodetic and seismological data in SW Taiwan are analysed and discussed in terms of present-day tectonic escape occurring in response to the active N100° collisional shortening. The escaping area corresponds to the onland extension of the Manila accretionary wedge; this region comprises a rheologically weak, thick muddy cover which is decoupled from the underlying basement by a décollement and which deforms mainly by aseismic creep. It is separated from the northern actual collisional area by a major WNW- to NW-trending structural and kinematic transition zone oblique to the structural grain of the belt, the Chishan Transfer Fault Zone. Geodetic data are further used to define several poorly deforming blocks undergoing nearly uniform displacement velocities and bounded by kinematic discontinuities that fit the major faults, and to determine the present-day across-strike and along-strike motions on these major faults. Although direct onland structural evidence of tectonic escape is poor, reconstruction of Quaternary paleostress patterns demonstrate that this escape probably began during the late Pleistocene, later than in northeastern Taiwan as a result of the southward migration of the collision through time. Offshore structural data help to constrain the geometry and the southern extension of the escaping blocks. Finally, a tentative model of lateral extrusion in SW Taiwan is proposed.

Keywords: Taiwan; GPS; tectonic escape; transfer fault zone

1. Introduction

The Taiwan mountain belt is an active orogen that results from the late Cenozoic oblique collision between the Luzon arc belonging to the Philippine Sea plate and the Chinese passive margin of the Eurasia plate (e.g. Suppe, 1984; Ho, 1986; Barrier and Angelier, 1986; Tsai, 1986; Teng, 1990). This collision segment connects the Ryukyu subduction zone, where the Philippine Sea plate is subducting beneath the Eurasian plate, and the Manila subduction zone, where the Philippine Sea plate is overriding the crust of the South China Sea (Fig. 1).

Because of the oblique (N054°W-directed) convergence of the Philippine Sea Plate toward the N060–070°E trending Chinese passive margin (Seno et al., 1993; Yu et al., 1997), and the consequent southward migration of the arc–continent collision through time, the Taiwan region exhibits from south to north all the stages of the collision process (Fig. 1): subduction in the Manila trench, incipient collision south of Taiwan, active collision in south-central Taiwan, past collision in the northern part (Lallemand and Tsien, 1997). Taiwan thus constitutes a natural laboratory to study the entire life of the collision by simply moving from SW to NE along the convergent Philippine–Eurasia plate boundary (Fig. 1).

Many geological studies have been devoted to the analysis of structures and deformation related to the

* Corresponding author.
E-mail address: lacombe@lgs.jussieu.fr (O. Lacombe).

0040-1951/01/$ - see front matter
PII: S0040-1951(00)00281-X

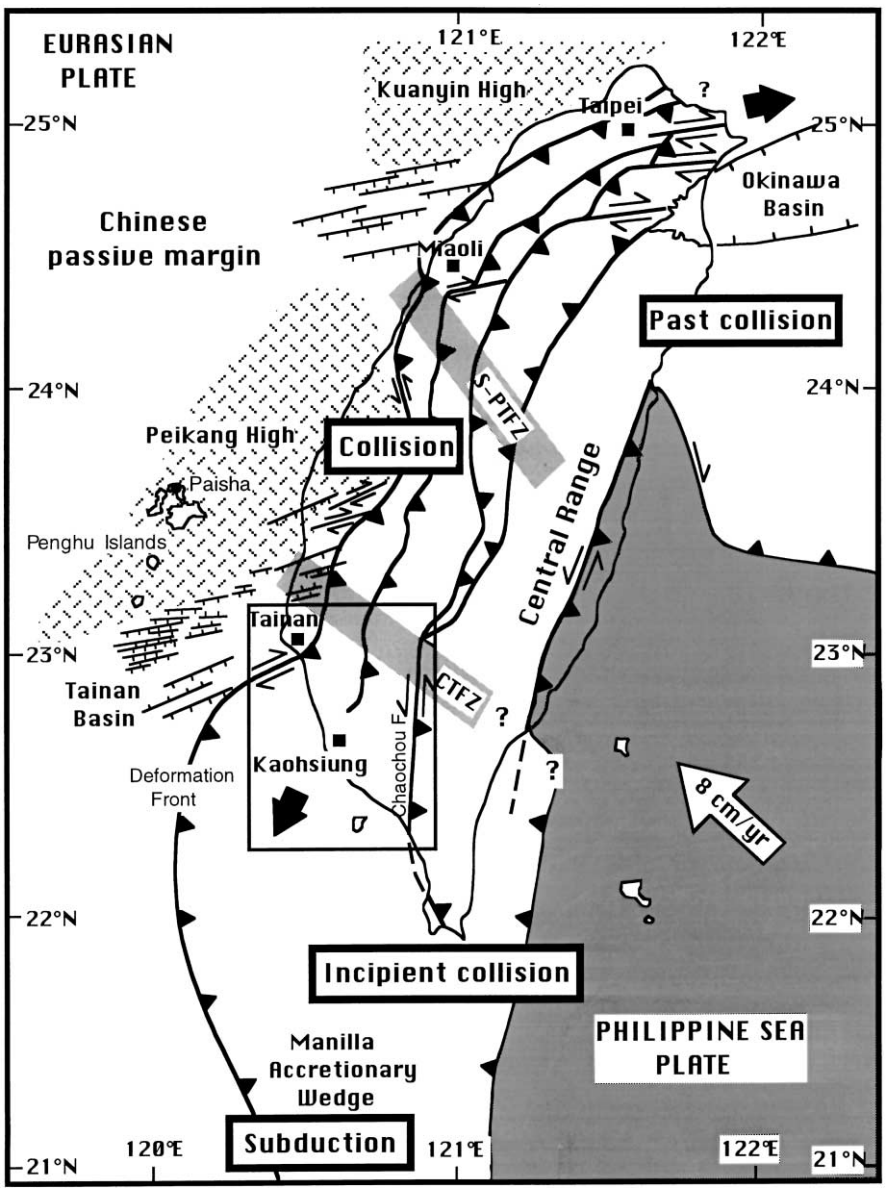

Fig. 1. Geotectonic setting and main structural features of Taiwan. The large open arrow shows the present direction of convergence of the Philippine Sea plate (dark grey) relative to South China; velocity after Yu et al. (1997, 1999). Heavy lines indicate major thrusts, triangles on upthrown side; lines with double arrows indicate major wrench faults. Hatched areas correspond to basement highs of the Chinese margin which underlie the deposits of the foreland basin. Large black arrows indicate tectonic escape at the tips of the belt. The frame shows the location of the area investigated.

active Taiwan collision. Sedimentological and structural fieldwork combined with new geophysical investigations onshore (Wu et al., 1997) as well as offshore Taiwan (e.g. Lallemand et al., 1997; Lundberg et al., 1997; Liu et al., 1997) have provided new insights into the timing and the overall signature of the collision, from local to lithospheric scales, allowing improved geodynamic models of the Taiwan collision

to be proposed (e.g. Huang et al., 1997; Malavieille, 1999). Recent GPS surveys over the years 1990–1995 (Yu et al., 1997, 1999) additionally provided a complete displacement velocity field of the Taiwan–Luzon area, bringing tighter constraints on the plate kinematics setting of the Taiwan collision and leading to a better characterisation and understanding of the short-term crustal deformation and mechanical behaviour in this active mountain belt.

The SW region of Taiwan has received particular attention because it corresponds to a key region to understand how the offshore Manila subduction and related accretionary wedge evolves northwards to the Taiwan oblique collision. Recent geological studies have focused on the geometry and the Plio-Pleistocene structural and kinematic evolution of the fold-and-thrust units of the southwestern Foothills (e.g. Lu, 1994; Lacombe et al., 1999; Hung et al., 1999; Mouthereau et al., 2001b). Based on sandbox modelling experiments, Lu and Malavieille (1994) and Lu et al. (1998) proposed that SW Taiwan was undergoing tectonic escape toward the SW: this escape occurs in response to both ongoing collisional shortening and local indentation by a basement high of the Chinese margin, the Peikang High (Fig. 1) acting as a buttress for the advancing thrust units and localising along its southern edge a large dextral transfer zone along which the structures were dragged to the SW.

The concept of tectonic escape (or tectonic extrusion) is referred to the lateral motion of structural units toward a free boundary in response to collisional shortening. Its application in SW Taiwan deserves discussion, because it is usually considered over larger areas and generally occurs at crustal–lithospheric scales along major transcurrent faults (e.g. SE Asia — Tapponnier et al., 1983; Turkey — Sengör et al., 1985; Eastern Alps — Ratschbacher and Merle, 1991). The goal of this paper is to examine recent geodetic, seismological and structural data in order to define the present-day kinematics of thrust units in SW Taiwan. This integrated study will lead us to provide further evidence for recent and present-day escape tectonics accompanying the ongoing collisional shortening in this area. We further aim at proposing a new model of lateral extrusion of the sedimentary cover decoupled from the deeper crustal levels.

2. Structural setting of SW Taiwan

The SW Taiwan area corresponds to the southern part of a Plio-Pleistocene foreland basin, which developed in response to lithospheric flexure due to the tectonic loading of the Central Range. The thick Plio-Pleistocene sediments of the foredeep were deformed and partially exposed due to the westward propagation of the collision. The western Foothills of Taiwan consists of a series of stacked west-vergent folds and thrust sheets resulting from the late Cenozoic collisional shortening (Lacombe et al., 1999; Mouthereau et al., 2001b). This deformation decreases toward the still slightly deformed western Coastal Plain.

Beneath the Pliocene–Pleistocene deposits which correspond to the sedimentary record of the collision, the Chinese margin and the Coastal Plain display series of ENE-oriented Miocene horsts and basins inherited from the opening of the South China Sea. The prominent Peikang High (Fig. 1) represents the shallow pre-Tertiary Chinese continental basement; it is characterised by a nearly semi-circular geometry convex toward the east and its southern edge is mainly controlled by ENE–WSW to E–W normal faults. The pre-collisional Tainan basin (Fig. 1) is located on the southern edge of the Peikang High; it is filled by thick clastic deposits of the Chinese passive margin.

The structural inhomogeneity of the Chinese margin as well as the obliquity of the collision have played a major role in the structural style of the Foothills, resulting in an along-strike variation of thrust wedge geometry and structural style of the frontal units (Lu et al., 1998; Mouthereau et al., 2001a). The Miocene extensional structures of the eastern part of the Tainan basin underwent compressional reactivation (and even inversion) during the arc–continent collision, indicating that in this area, both the sedimentary cover and the basement were involved in collisional shortening. This area of basement-involved tectonics is limited to the south by a major oblique fault zone trending WNW–ESE to NW–SE which probably corresponds to an ancient transfer fault inherited from the rifting period: the Chishan Transfer Fault Zone (CTFZ) (Fig. 1). Reactivation of such a pre-existing discontinuity during the Plio-Pleistocene collision resulted in localising a major transfer fault zone in the cover which guided

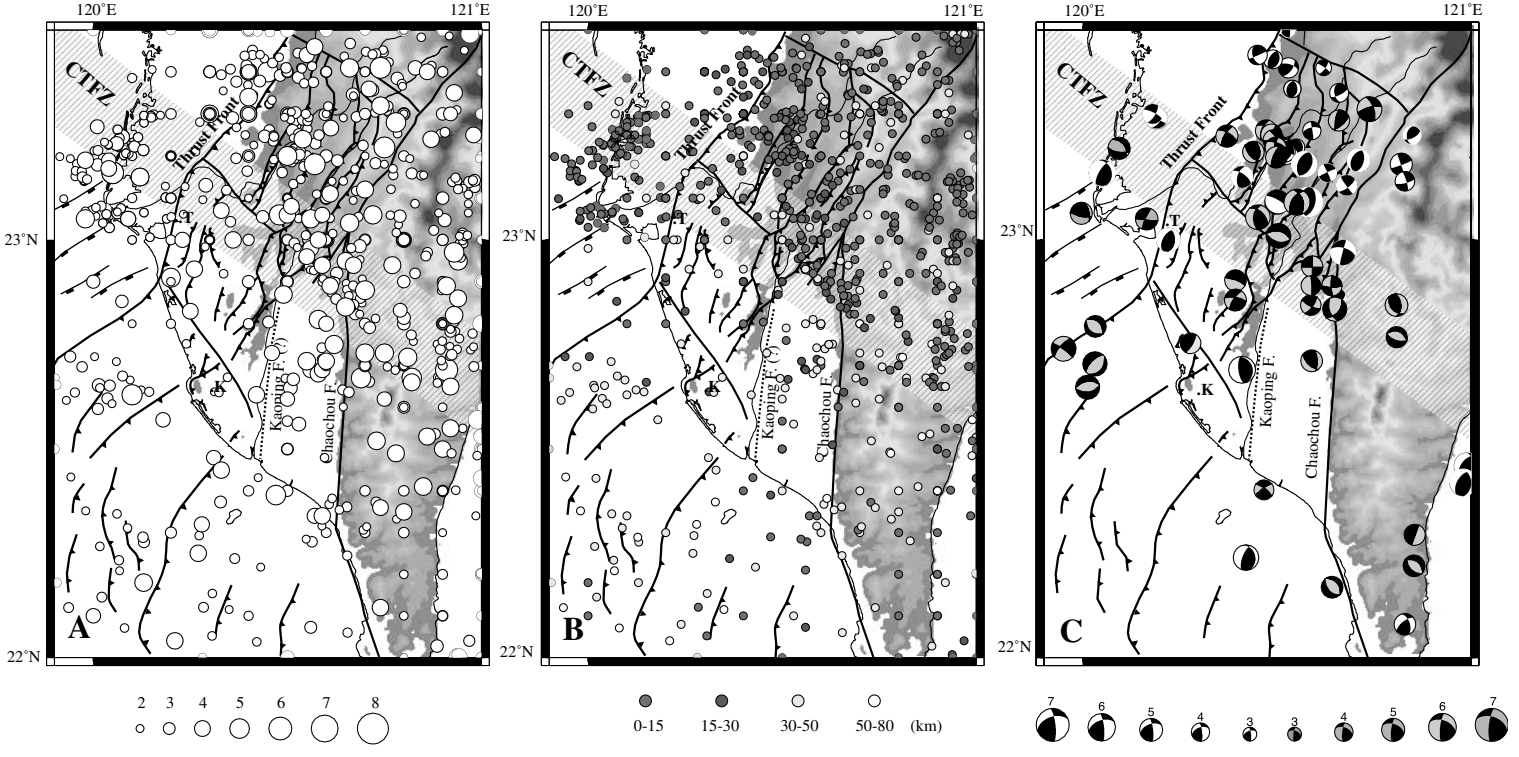

Fig. 2. Seismicity in southern Taiwan over the years 1900–1998 (source: Central Weather Bureau, Taiwan; USGS; CMT Harward). (A) Earthquake distribution as a function of magnitude. Note the low seismicity and the low earthquake magnitude in SW Taiwan. (B) Earthquake distribution as a function of focus depth. North of the Chishan Transfer Fault Zone (CTFZ, hatched area), 0–30 km depth foci are numerous and related to actual collisional setting; south of the CTFZ, most earthquakes occur at depth larger than 25 km, which suggests that the upper crust, comprising the sedimentary wedge, mainly deforms by aseismic creep. (C) Earthquake focal mechanisms (dilatational first motion quadrants in white: after Rau and Wu (1998) for magnitudes lower than five; after Harward for magnitudes larger than five; dilatational first motion quadrants in grey: after Yeh et al. (1991).

thrust emplacement (Deffontaines et al., 1997; Lacombe et al., 1999).

In contrast, the collisional deformation in the western part of the Tainan–Kaohsiung province investigated herein did not involve the pre-Miocene basement, and is mostly restricted to the thick sedimentary cover. The propagation of frontal thrust units probably occurred above a low-dipping and shallow décollement surface above the pre-Miocene basement: structures consist of regularly spaced fault-propagation folds and pop-up structures, which usually develop in relation to flat detachments with low-friction conditions (e.g. Davis et al., 1983; Huiqi et al., 1992), such as for accretionary wedges. This deformation style is therefore largely controlled by high fluid pressure conditions, as shown by the presence of the thick poorly consolidated muddy Quaternary deposits and numerous mud volcanoes. This indicates that this province can be regarded as the onshore extension of the submarine Manila accretionary wedge (Sun and Liu, 1993; Liu et al., 1997), so that the thrust wedge front defined onland can be correlated with the offshore northern extension of the Manila trench (Fig. 1).

3. Seismicity in SW Taiwan

Fig. 2 shows the distribution of earthquake epicenters in SW Taiwan as a function of magnitude (Fig. 2A) and focus depth (Fig. 2B). The SW Taiwan region can thus be divided into two sub-areas, north and south of the CTFZ. This fault zone constitutes a clear transition zone north of which shallow earthquakes (0–30 km) are abundant and related to collisional shortening. To the south, shallow earthquakes are scarce and small in magnitude (Fig. 2A); the serial E–W seismic sections of Fig. 3 (Wu et al., 1997) highlight this lack of shallow seismicity between 0 and 20–25 km (sections C–C′ to G–G′); earthquakes occur at larger depths, between 25 and 50 km.

We thus consider the CTFZ as a major seismotectonic transition zone, increasing its importance and extent previously defined by Deffontaines et al. (1997) based on morphological evidence and field mapping. The CTFZ is underlined by a line of earthquakes ranging in depth between 50 and 80 km which clearly connects to the earthquakes evidenced beneath the Central Range (Fig. 2B). The striking contrast in earthquake occurrence to either side of the CTFZ (Fig. 2) confirms that this transition area separates two different tectonic domains. In the northern area, actual collision occurs (Fig. 3, sections A–A′ and B–B′); the southern region rather corresponds to the onland extension of the Manila accretionary wedge, where shortening occurs while the deformation front moves westward toward the continental shelf of Eurasia. In detail, earthquake focal mechanisms (Yeh et al., 1991; Rau and Wu, 1998) suggest that the CTFZ presently corresponds to a major crustal–lithospheric left-lateral wrench boundary (Fig. 2C).

South of the CTFZ, inspection of the earthquake distribution also reveals a clear across-strike contrast in seismicity between the poorly seismic area west of the Kaoping river and the area east of this river (Figs. 2A and B). In the seismic sections C–C′ to F–F′ (Fig. 3), the low seismicity zone previously identified ends abruptly to the east along the N–S boundary which effectively fits the course of the Kaoping river. Although such a boundary between regions of seismic activity and inactivity needs not be a fault, and may for instance reflect a strong rheological transition, it is more likely that a fault exists (at least at depth) along this morphological lineament. As a consequence, although speculative because of the poor geological evidence, we propose to define this apparent seismological boundary as a "Kaoping Fault" (Figs. 2 and 3).

4. Earthquake focal mechanisms in SW Taiwan

Fig. 2C shows the distribution of reconstructed earthquake focal mechanisms from Rau and Wu (1998) at depths of about 10–20 km and those published by Yeh et al. (1991) which have been reported on the same map. We have focused mainly on earthquake data by Rau and Wu, because foci have been precisely relocated. We have used this set of data including 48 focal mechanisms of well located crustal earthquakes in the area between 22.3°N–24.7°N in latitude and 120.2°E–121.4°E in longitude in order to define the present-day crustal stress. From this set we extracted a subset of 37 earthquakes in the area of interest in this paper, between 22.86°N–23.89°N in latitude and 120.18°E–120.79°E in longitude

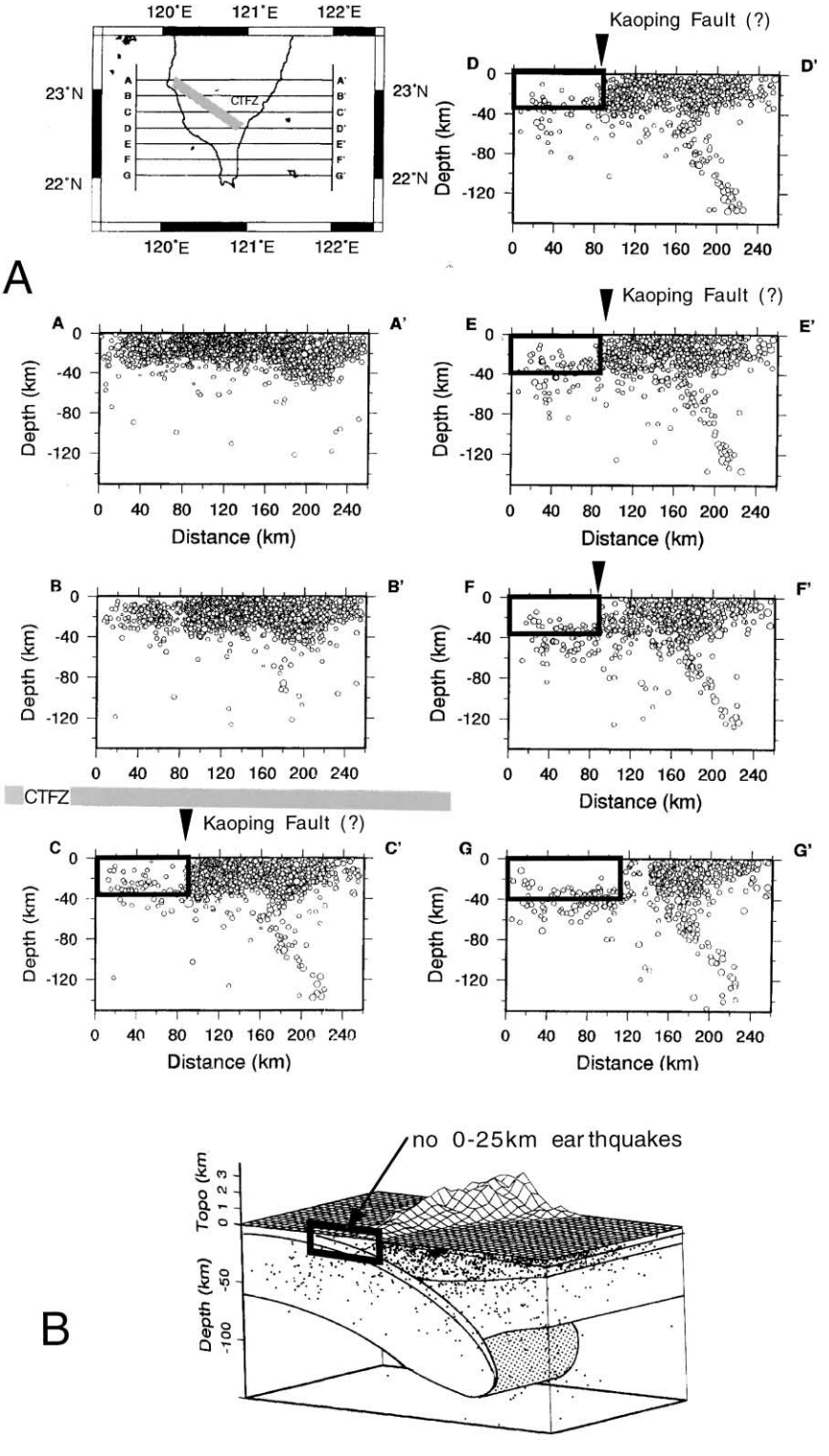
A
120°E
121°E
122°E
23°N
22°N
CTFZ
Kaoping Fault (?)
Depth (km)
Distance (km)
0 40 80 120 160 200 240
0 -40 -80 -120
CTFZ
B
no 0-25km earthquakes
Topo (km
0 1 2 3
Depth (km)
-50
-100

Table 1
Characteristics of earthquake focal mechanisms used from stress calculation in the area investigated (data after Rau and Wu, 1998; inversion after Angelier, 1998) (Lon, Lat: Longitude, Latitude in degrees; Strike, Dip and Rake for each nodal plane, in degrees; depth in km. Most of the mechanisms (31) are consistent with the calculated stress tensor (last line of the table: trend and plunge of each principal stress axis, in degrees; Φ ratio $= (\sigma 2 - \sigma 3)/(\sigma 1 - \sigma 3)$). The mechanisms in italics (5) are of normal and normal–oblique types, inconsistent with the dominant compressional stress regime. The bold mechanism is inconsistent with both regimes.

Lon.	Lat.	Strike 1	Dip 1	Rake 1	Strike 2	Dip 2	Rake 2	Depth
120.78	23.77	352	29	58	207	66	106	23.52
120.77	23.87	326	56	53	199	48	132	27.17
120.75	*23.88*	*29*	*85*	*−80*	*145*	*11*	*−154*	*12.69*
120.75	23.88	228	90	80	138	10	−180	13.08
120.75	23.87	336	61	73	189	33	118	25.8
120.75	23.82	207	72	64	85	32	144	16.64
120.74	23.89	228	90	80	138	10	−180	12.61
120.73	*23.89*	*234*	*21*	*−44*	*6*	*76*	*−106*	*13.37*
120.72	*23.89*	*257*	*57*	*−66*	*38*	*40*	*−122*	*12.97*
120.72	*23.88*	*263*	*60*	*−55*	*28*	*45*	*−135*	*12.58*
120.72	*23.87*	*354*	*47*	*−69*	*145*	*47*	*−111*	*13.28*
120.71	23.19	12	51	77	212	41	105	13.84
120.68	23.56	112	55	84	302	35	99	13.15
120.68	23.13	144	85	19	52	71	175	5.91
120.67	22.97	286	60	3	194	88	150	18.92
120.66	23.35	169	50	23	64	73	138	14.99
120.65	22.86	192	56	53	66	48	132	17.65
120.63	23.16	335	88	5	245	85	178	9.46
120.62	23.41	304	82	−18	37	72	−171	3.38
120.61	23.63	181	85	30	88	61	174	14.64
120.59	23.26	351	85	30	258	61	174	11.19
120.55	23.22	144	71	74	5	25	128	16.85
120.54	23.36	358	41	75	198	51	103	12.71
120.54	23.36	3	56	78	204	36	107	12.96
120.53	23.5	353	76	43	250	48	161	14.5
120.53	**23.41**	**35**	**60**	**35**	**286**	**60**	**145**	**6.98**
120.52	23.21	205	45	83	35	45	97	13.88
120.52	23.21	106	85	80	350	11	154	14.96
120.51	23.22	318	78	28	222	63	166	15.02
120.49	23.72	279	60	−19	19	73	−149	21.87
120.49	23.43	18	35	81	208	55	96	6.05
120.45	23.44	159	50	4	66	87	140	11.07
120.43	23.52	159	55	−3	251	87	−145	16.15
120.41	23.15	305	66	39	197	55	150	19.43
120.19	23.29	301	69	−22	39	69	−158	16.35
120.19	23.29	119	87	35	27	55	177	14.3
120.18	23.3	296	76	−21	32	70	−165	18.72
	$\sigma 1$		$\sigma 2$		$\sigma 3$		Φ	
	277 08		185 09		048 78		0.15	

Fig. 3. Earthquake distribution with depth in southern Taiwan (after Wu et al., 1997). (A) Serial E–W seismic sections in southern Taiwan. Note the signature of the collision north of the CTFZ, and the striking lack of shallow seismicity south of the CTFZ, in the area which corresponds to the northern extent of the Manila accretionary prism (frame). Note also the abrupt end of the aseismic area to the East along the inferred "Kaoping Fault". (B) Lithospheric-scale block diagram of the subduction in southern Taiwan.

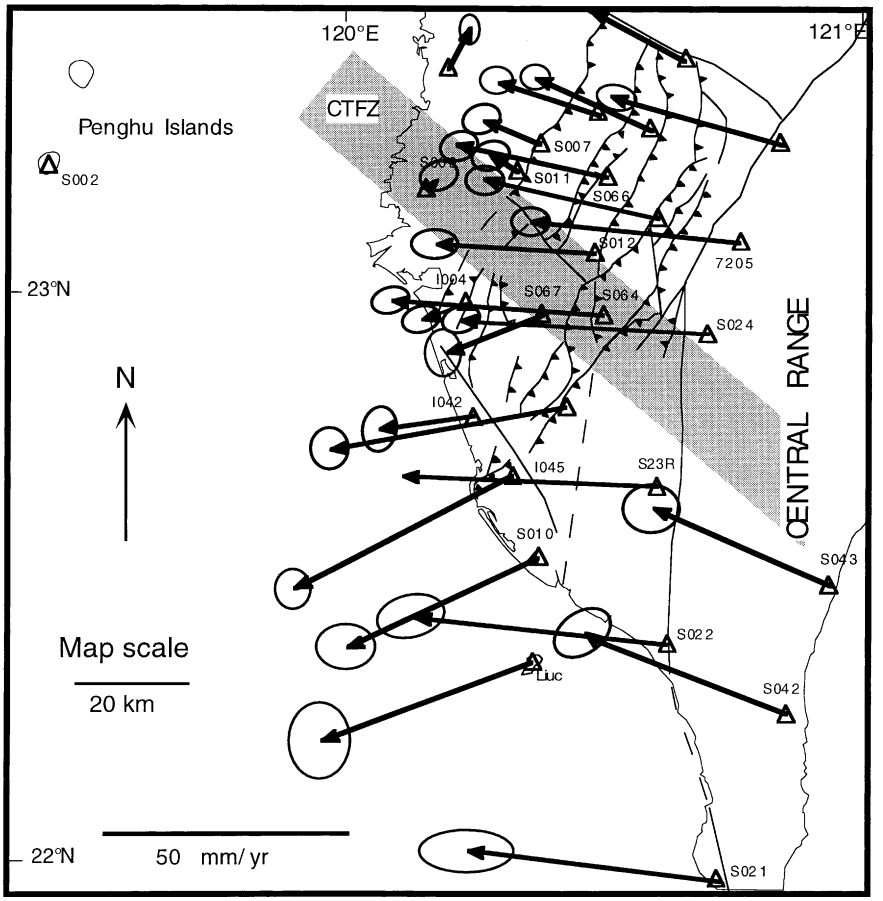

Fig. 4. GPS displacement velocity field in the area investigated (Yu et al., 1997), relative to Paisha (Penghu islands, see Fig. 1). Triangles: GPS stations. Black arrows connected to triangles: displacement vectors, length proportional to velocity. The 95% confidence ellipse is shown at the tip of each velocity vector. Note the southwestward present-day displacement south of the CTFZ, suggesting tectonic escape.

(Fig. 2C). This area, located north of the CTFZ, corresponds to part of the southwestern Foothills and the adjacent portions of the Coastal Plain and the Central Range. To determine the regional seismotectonic regime, we use a method defined by Angelier (1998) and derived from earlier direct inversion techniques (e.g. Angelier, 1990), which does not require any choice of a nodal plane.

Among the subset of 37 earthquakes, 31 focal mechanisms, reverse, strike-slip and oblique-slip in type, allowed reconstruction of a regional stress regime. The minimum stress axis obtained is nearly vertical (it plunges 78°), whereas the maximum compressive stress axis is nearly horizontal (it plunges 8°) and trends N97°E (Table 1). The ratio Φ between the principal stress difference is 0.15, indicating that the minimum and intermediate principal stresses have rather close values with respect to the maximum principal stress. For the nodal planes that best fit the solution tensor, the angle between the vectors of actual slip and computed shear stress averages 25°. Although this misfit is large, it remains acceptable considering the size of the area considered (where the seismotectonic state of stress is certainly not homogeneous) and the amount of uncertainties in the determination of focal mechanisms.

Separate determination was made with the focal mechanisms closer to the strike-slip type (16 earthquakes) and to the reverse type (15 earthquakes). They yielded very similar results: the maximum stress

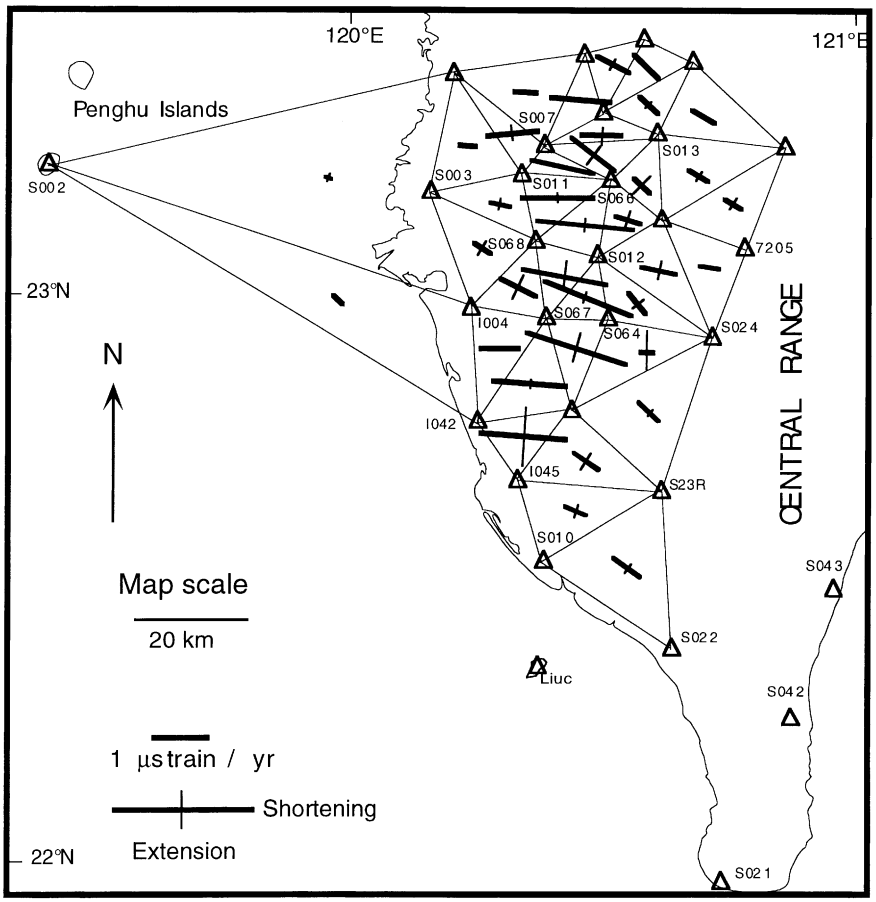

Fig. 5. Principal strain rates within GPS subnets in southwestern Taiwan (Yu and Chen, 1998). Heavy lines: strain axes in the area investigated, length proportional to magnitude (see scale).

is nearly horizontal and trends N94°E and N105°E, respectively. Although this separation obviously resulted in better misfit levels (with angles of 19 and 11°), the similarity between the trends of compression strongly suggests that the 31 reverse, strike-slip and oblique-slip focal mechanisms in fact correspond to a single seismotectonic regime dominated by N97°E compression. Among the six remaining focal mechanisms, five are compatible with a regime of normal and normal–oblique type; but this subset is too small to be considered as reliably reflecting a second regionally significant state of stress.

Thus, our calculation of the present-day crustal stress north of the CTFZ is in general agreement with previous determinations of the Pleistocene and present-day directions of compression across the collision belt of southern Taiwan (e.g. Suppe et al., 1985; Angelier et al., 1986; Lacombe et al., 1999). The few mechanisms south of the CTFZ (Fig. 2C) are also consistent with a nearly E–W compression (although too few to allow inversion), which indicates that the crust of SW Taiwan north and south of the CTFZ is mechanically coupled with the inner belt and the colliding indentor (the Luzon arc) and is undergoing collisional shortening. In contrast, the uppermost part of the crust south of the CTFZ, comprising the accretionary wedge, apparently deforms mainly by aseismic creep. Some mechanisms (Yeh et al., 1991) indicate right-lateral motion along NE-trending structures, especially along the frontal thrust zone and the Chishan fault zone if correctly located (Fig. 2C), but focus depths are not precisely constrained.

5. Present-day kinematics of SW Taiwan inferred from GPS data and evidence for tectonic escape

Recent GPS surveys have provided the first complete displacement velocity field of the Taiwan area (Yu et al., 1997, 1999). In contrast to the ITRF96 frame used by Yu et al. (1999), the GPS network adopted in the present study involves a fixed local frame, where the Paisha station of the Penghu islands (Fig. 1) and the azimuth from Paisha to Taipei (52.1°) are considered fixed (Yu et al., 1997) (Fig. 4). It is justified since Paisha is attached to the South China shelf and the motion of Taipei relative to this shelf is very small: between 1991 and 1995, the average rates of change on the north and east components of the baseline between the two permanent Paisha and Taipei GPS stations were only 0.3 ± 0.2 mm/yr and 1.6 ± 0.4 mm/yr, respectively (Yu et al., 1997). This study revealed a N054°W directed motion and a velocity of about 8 cm/yr of the Philippine Sea plate relative to South China (Yu et al., 1997). The main source of the difference between kinematic estimates by Yu et al. (1997) and Seno et al. (1993) lies in the eastward displacement of the South China block with respect to stable Eurasia, about 1 cm/yr (Yu et al., 1999).

GPS displacement velocities display two main trends of variation in the area investigated (Fig. 4): (1) they decrease westwards north of 23°N; and (2) they increase southwards in the western part of the studied region. A possible interpretation of these kinematic variations is that for short inter-seismic periods the situation is more locked north of the CTFZ, in the collision area in front of the Peikang High, than south of the CTFZ where collision is only at an incipient stage. To the north, elastic strain accumulation is therefore more important than to the south where mechanical decoupling still prevails and allows easier permanent deformation. This is consistent with geological evidence concerning the superimposed effects of the obliquity of the collision and the geometry (salients and reentrants) of the Chinese margin.

In terms of velocity vector trends, there is also a strong contrast in kinematics between central and SW Taiwan: GPS stations are moving toward the west in central Taiwan, whereas in the Kaohsiung coastal area, the displacement vectors display a clear counterclockwise deviation toward the SW. This deviation appears just south of the CTFZ (Fig. 4), a major present-day kinematic boundary. Strain orientations and magnitudes calculated from the GPS data in this region (Fig. 5) indicate an average N100–110° shortening (Yu and Chen, 1998).

5.1. Do GPS data reflect long-term deformation?

The actual significance of GPS data in terms of permanent deformation, and hence their use as a reliable tool to draw geological conclusions about collisional shortening or lateral escape, certainly deserves discussion. At the scale of the Taiwan island, the deformation tensors derived from geodetic data display a fan-shaped distribution of shortening axes (Yu and Chen, 1996). In most areas, and in particular in our study region, these axes are colinear with long-term permanent deformation patterns deduced from Quaternary faulting (e.g. Angelier et al., 1986; Lacombe et al., 1999). Furthermore, joint analyses of magnetic susceptibility anisotropy and brittle tectonics indicate that Quaternary deformation was dominated by average N100°–110° shortening in southwest Taiwan (Lee and Angelier, 1995). As a result, this good qualitative agreement between axes of short-term and long-term deformation tensors suggests that the present-day geodetic deformation trends reflect long-term collisional deformation trends.

The present-day shortening rates determined from GPS studies (Fig. 5) are however much larger than the finite shortening rates calculated for the Plio-

Fig. 6. Present-day block kinematics in SW Taiwan inferred from GPS data. (A) Definition of poorly internally deforming blocks undergoing present-day uniform displacement velocity and limited by kinematic discontinuities fitting with major structural features. Each arrow represents the average velocity vector of each block. (1), (2), (3), (4): major blocks, see text. (B) Across-strike (fault-perpendicular) components of motion of selected stations belonging to the previously defined blocks. (C) Along-strike (fault-parallel) component of motion of selected stations belonging to the previously defined blocks. (D) Present-day motion along major discontinuities in SW Taiwan. 1 — Right-lateral motion along deformation front, consistent with structural data and previous interpretations. 2 — Reverse-left lateral motion along the inferred "Kaoping Fault" deduced from GPS data (triangles on upthrown side). 3 — Normal-left lateral motion along the Chaochou Fault deduced from GPS data (barbs on downthrown side).

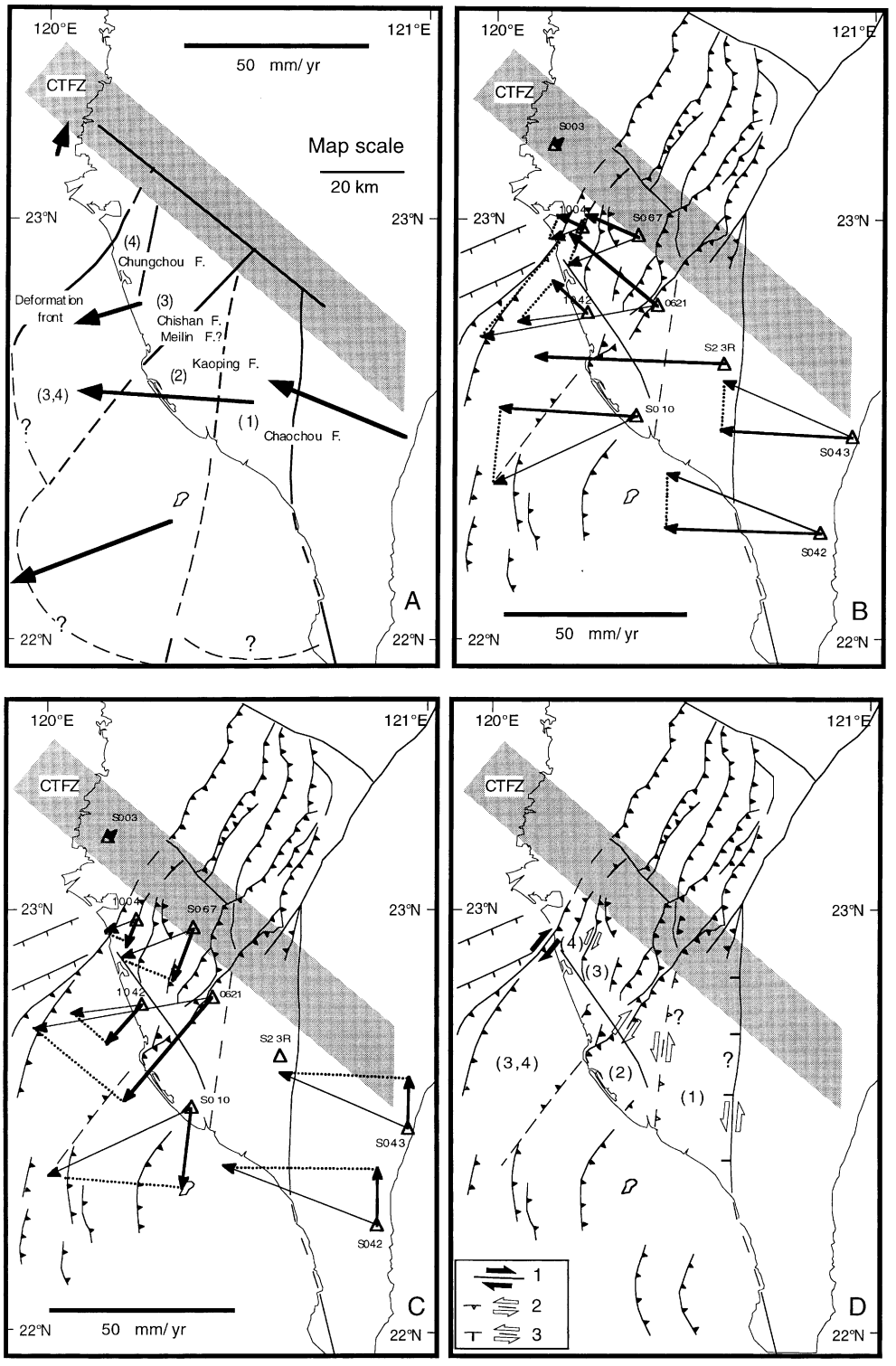
120°E
121°E
50 mm/yr
CTFZ
Map scale
20 km
23°N
22°N
(4)
Chungchou F.
Deformation front
(3)
Chishan F.
Meilin F.?
Kaoping F.
(2)
(3,4)
(1)
Chaochou F.
?
A
S003
1004
S067
1042
0621
S23R
S010
S043
S042
B
C
D
1
2
3

Pleistocene geological periods (Mouthereau et al., 1996). In a first approximation, elastic strain accumulates between seismic events as a result of locking of thrust zones, and is instantaneously released during earthquakes. During major earthquakes, most of the large co-seismic displacement occurring across the front thrusts of the belt is absorbed in the interior of the mountain belt while the convergence velocity of the two plates remains constant. During the periods between major earthquakes (which is the case for the GPS survey used), elastic deformation occurs, and should be substracted from the total deformation observed to obtain the permanent deformation over the same period (e.g. Le Pichon et al., 1998). We consider that this provides a possible explanation for the discrepancy between the GPS-based instantaneous shortening rates and the finite ones based on consideration of much longer periods.

As a consequence, if a large amount of plate convergence is absorbed by transient elastic strain across the collision zone during inter-seismic periods, it must be accommodated in major thrust zones during large earthquake crises. To this respect, the recent Chichi earthquake (21 September 1999), although having occurred north of the area under interest, deserves consideration not as a simple thrust earthquake within a deforming collision belt, but maybe as the main expression of the shear at the plate interface. In SW Taiwan, however, the proportion of elastic strain accumulation is probably much less than north of 23°N as discussed before.

It is worthwhile to notice that despite the likely elastic strain accumulation, local surveys (Angelier et al., 1997) have shown that between 1982 and 1995 the single Chihshang Fault in the Longitudinal Valley of eastern Taiwan accommodated more than one fourth of plate convergence by aseismic creep. This explains that despite the high average rate of motion across this fault zone, the frequency and importance of earthquakes are much less than could be expected, even though forthcoming locking of the thrust zone and further strain accumulation cannot be excluded.

The low magnitude of the few shallow (0–25 km) earthquakes (Fig. 2) suggests that the investigated SW Taiwan area (south of 23°N) is mostly undergoing aseismic creep, at least above the décollement at the base of the neogene sedimentary pile. We infer that coupling and subsequent elastic strain accumulation remain low. Although the strain deduced from five years of GPS data indicates higher shortening rates than the geological evidence, we consider that most of this strain nevertheless reflects the type and trends — if not the amounts — of long-term deformation. The GPS displacement field can thus reliably be used to infer the overall present-day block kinematics of SW Taiwan, at least in terms of orientations.

Another point that deserves discussion concerns the significance of geodetic deformation in terms of crustal deformation when geodetic stations are located in a sedimentary accretionary wedge at least partially decoupled from the deeper basement by a décollement surface. The significance of displacement velocity vectors in such stations may greatly differ from that of the stations located within the inner part of the belt, which reflects more reliably crustal movement. It is the case of SW Taiwan south of the CTFZ, where velocity vectors may reflect the movement of the sedimentary cover without implying a similar behaviour of the entire crust.

5.2. Present-day kinematics of SW Taiwan: shortening and lateral escape

We conducted a simple planar kinematic reasoning in order to define the present-day kinematics of SW Taiwan (Fig. 6). Although certainly less rigorous than the spherical geometry commonly used to depict plate kinematics, it is nevertheless valid considering the small size of the area investigated and the uncertainties; it additionally provides results similar to that obtained on the sphere (Angelier et al., 1999).

In addition to the general southward deflection of GPS displacement velocity vectors south of the CTFZ (Fig. 4), a closer inspection of GPS data suggests that nearly rigid (or moderately deforming) blocks undergoing almost uniform displacement can be defined in the first approximation (Fig. 6A). The large spacing of the GPS stations and the small number of velocity data available to define each block (see below) do not allow an accurate quantitative comparison between the variation in velocity within a block and the variation in velocity between blocks in order to support our assumption. However, as Figs. 4 and 7A and B suggest, the variations in velocity within the individual blocks (differences between station

velocity vectors) remain generally of the same order than the uncertainty on the individual velocity vectors; they also remain much lower than changes in velocity between blocks. It is thus worthwhile to consider that the inferred block boundaries constitute abrupt discontinuities in GPS displacement field. Relative variations are large in azimuth between Central Range and block 1 and between blocks 1 and 2, and in velocity between blocks 2 and 3 and between blocks 3 and 4 (Fig. 7B). This suggests than even though the assumption of nearly rigid blocks must be considered carefully, especially for block 2 that displays the greatest dispersion (Section 5.3), the internal deformation of blocks remains limited compared to that accommodated along block boundaries. In addition, it is noteworthy that these inferred block boundaries fit very well the known structural features (see Fig. 6).

We consequently consider different blocks limited by major structural discontinuities which are (Fig. 6A): the Chaochou Fault, the inferred "Kaoping Fault", the Chishan Fault, extended to the thrust fault north of Kaohsiung (southern extent of the Meilin Fault); and the frontal thrust fault (deformation front) which limits the pop-up structures near Tainan city and which connects offshore with the right-lateral transfer zone south of the Peikang High (Liu et al., 1997). Finally, we propose to take into account the Chungchou Fault as a block boundary onland, albeit of second-order (Fig. 6A). The blocks thus defined are (Figs. 6A and 7A and B): the Kaoping–Chaochou block (1), limited by the Kaoping and Chaochou fault zones, and comprising two GPS sations (S23R and S022); the Kaohsiung–Fengshan block (2), limited by the Kaoping and the Chishan/south Meilin faults, and comprising four GPS stations (0621, I045, S010 and Liuc); the Meilin block (3), limited by the Chishan fault, the Chungchou fault and the CTFZ to the north, and comprising two GPS stations (S067 and I042); and finally the westernmost block, called the Tainan block (4), comprising the single I004 GPS station. The Central Range (stations S042 and S043) constitutes the reference eastern domain (Figs. 6A and 7), and the South China shelf is considered stable. Based on the assumption on rigid blocks, Fig. 6A shows the regional displacement pattern where each arrow represents the average velocity vector of each block (Angelier et al., 1999); the uncertainties are of the same order than those on each individual velocity vectors. Note that the clear change in azimuth of station displacement velocities across the inferred "Kaoping Fault" indirectly confirms the existence of a discontinuity which is likely to be a fault zone.

The displacement velocity pattern (Fig. 4) allows

Block	Stations	Lat (°)	Long (°)	V (mm/yr)	Azimuth (°)
Central Range	S042	22.2436	120.8468	42.7 ± 1.6	291.7 ± 1.7
	S043	22.4735	120.9269	36.0 ± 2.2	294.7 ± 2.0
1	S022	22.3683	120.6157	48.5 ± 2.2	276.3 ± 2.3
	S23R	22.6468	120.5981	49.0 ± 0.9	272.8 ± 0.9
2	0621	22.7915	120.4258	46.3 ± 1.4	260.3 ± 1.5
	I045	22.6694	120.3194	47.4 ± 1.8	243.4 ± 1.6
	S010	22.5254	120.3718	41.0 ± 2.8	245.4 ± 2.2
	Liuc	22.3427	120.3707	44.4 ± 2.9	250.7 ± 3.2
3	S067	22.9531	120.3759	19.4 ± 1.8	247.5 ± 2.1
	I042	22.7718	120.2446	18.0 ± 1.6	263.3 ± 1.6
4	I004	22.9753	120.2310	8.1 ± 1.7	250.4 ± 1.4

Fig. 7. (A) Displacement azimuths and velocities of stations defining blocks 1–4, as well as of the Central Range (reference) (after Yu et al., 1997). (B) Azimuth versus velocity diagram for station displacements within each block. The distribution of plots (stations) suggest that changes in velocity within blocks remain usually limited compared to changes in velocity between blocks. Note the clear change in azimuth between Central Range and block 1 and between blocks 1 and 2, and in velocity between blocks 2 and 3 and between blocks 3 and 4.

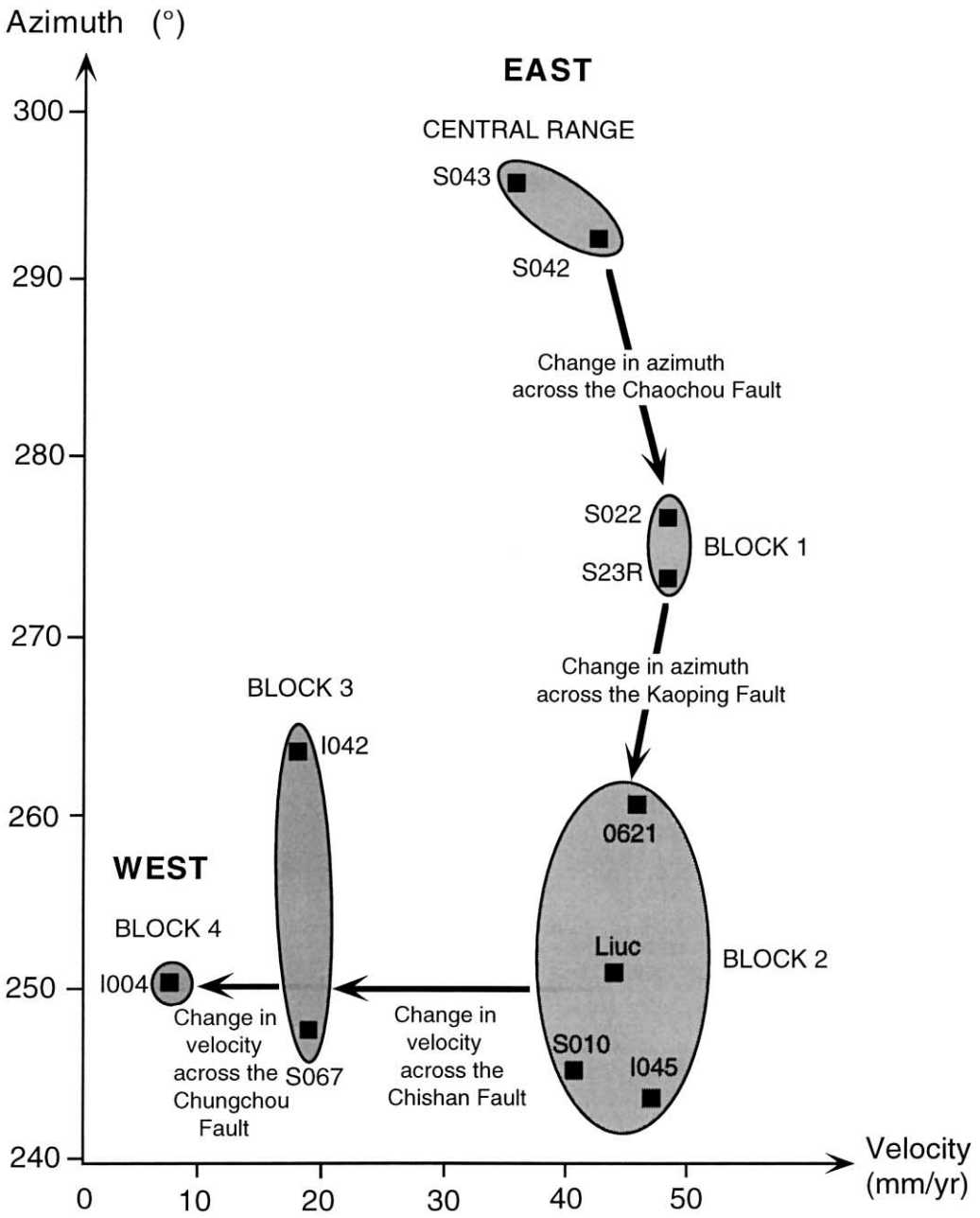

Fig. 7. (*continued*)

determination of the relative motion of these blocks along the previously defined discontinuities, by considering both the fault-perpendicular (across-strike) (Fig. 6B) and the fault-parallel (along-strike) components of motion (Fig. 6C) deduced from a couple of stations belonging each to one of the two blocks separated by the considered discontinuity. The across-strike component of motion deduced from GPS (Fig. 6B) suggests that most of the major discontinuities are undergoing shortening, except the Chaochou

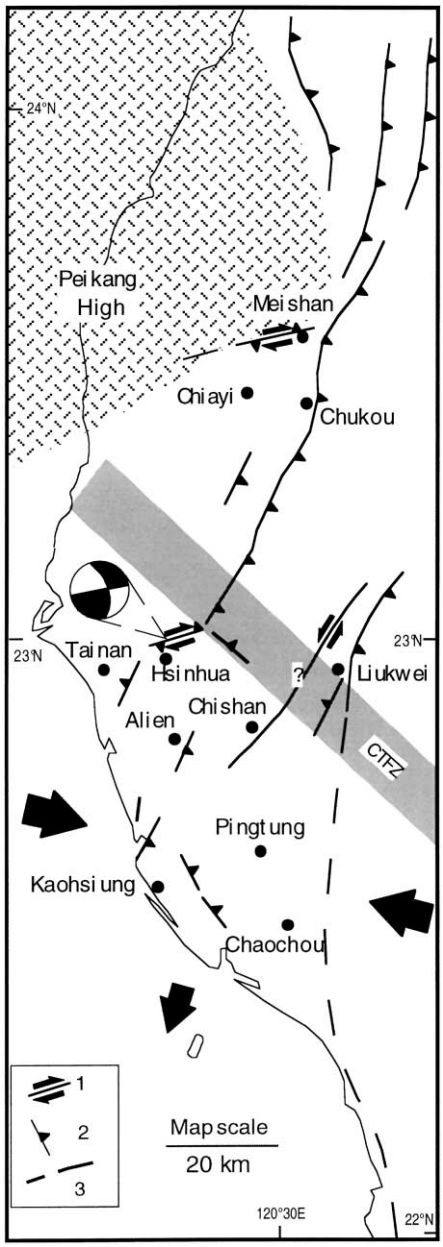

Fig. 8. Active faults in SW Taiwan (modified after Hsu and Chang, 1979). 1 — Active right-lateral/reverse motion along Meishan and Hsinhua faults and left-lateral motion along the Chishan fault. 2 — Active reverse fault motions. 3 — Inferred active fault. The large convergent black arrows indicate the average direction of shortening, the small arrow the subperpendicular direction of escape.

Fault which displays evidence of a dilatational component (Fig. 6D). This is consistent with field evidence that most of them correspond to still active thrust faults (Fig. 8).

Because this paper focuses on escape tectonics, the along-strike component of motion has received particular attention. GPS data are used herein to infer the relative along-strike motion of the previously defined blocks, and therefore the lateral component of motion along their boundaries (Fig. 6C). A southward movement of the Kaoping–Chaochou block (1) with respect to the Central Range is identified by comparison between stations S042–S043 and station S23R. Along the inferred Kaoping Fault, comparison between station S23R and stations 0621–S010 suggests that this fault zone is moving with a left-lateral component (Fig. 6D). The Kaohsiung–Fengshan block (2) is moving southwestward with respect to the Meilin block (3) along the Chishan Fault as deduced from comparison between stations 0621–S010 and stations I042–S067: this suggests a right-lateral component of motion along the Chishan Fault (Fig. 6D). The Meilin block (3) is also moving southwestward with respect to the Tainan block (4) along the Chungchou fault which consequently exhibits a right-lateral component of motion (comparison between stations S067 and I004) (Fig. 6D).

In this framework, the few ENE–WSW trends of maximum horizontal stress deduced from borehole breakouts (Suppe et al., 1985), which display counterclockwise deviation with respect to the overall N100° compression, could be interpreted as due to local stress reorientation of the present-day N100° compression along NE thrusts undergoing incipient right-lateral component of motion, consistent with the tectonic escape.

5.3. Comparison with active faulting in SW Taiwan

Active tectonics has been recognised since a long time in SW Taiwan. Bonilla (1975, 1977), Biq (1976) and Hsu and Chang (1979) reported active faults identified by morphological evidence. The main results are shown in Fig. 8.

First, active thrust motions occur along NE trends (Fig. 8), in agreement with present-day prevailing

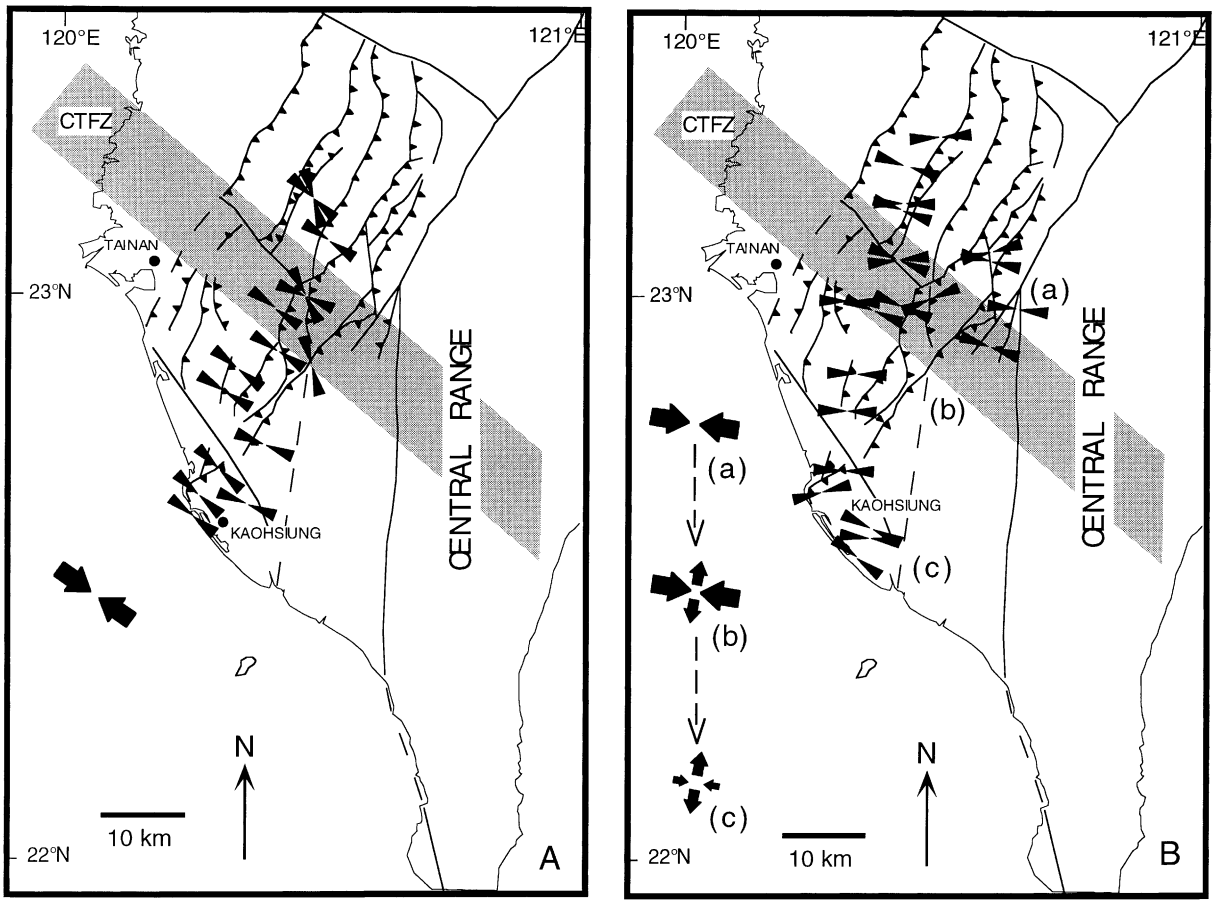

Fig. 9. Pleistocene stress patterns in southwestern Taiwan. (A) Pleistocene NW–SE compression. Convergent arrows indicate directions of $\sigma 1$ (data after Rocher et al., 1996; Mouthereau et al., 1998; Lacombe et al., 1999). The large black convergent arrows indicate the average regional compression. (B) Late (?) Pleistocene WNW–ESE to E–W compression. Note the along-strike change in the relative stress magnitudes (convergent arrows: compression, divergent arrows: extension) accompanying the regional E–W regional compression (a–c).

contraction: it is especially clear north of the CTFZ, but also south of the CTFZ, where most of active faulting has been reported along the inferred block boundaries. Note that a thrust component of motion is also identified along a NW–SE trend east of Kaohsiung, that is along the southern extent of the Fengshan Transfer Fault Zone (Deffontaines et al., 1997; Lacombe et al., 1999), which may reflect slight internal deformation of block 2 (Section 5.2). Second, evidence for right-lateral component of motion is provided by the Hsinhua fault, east of Tainan, whose corresponding focal mechanism is presented in Fig. 8, or the Meishan Fault, north of Chiayi. These fault motions reflect the compressional strike-slip reactivation of ENE trending normal faults of the Tainan basin in response to the collision.

Note that north of the CTFZ, the motion along some active faults remains rather consistent with a left-lateral slip along NE trends, as along the northern part of the Chishan fault: this motion is not consistent with the conclusions inferred from GPS studies. This emphasises again that the escape process is restricted to the area south of the CTFZ. This leads us to consider that despite similar orientation and sense of slip, the Meishan fault and the related earthquake rather reflect inversion of the Tainan basin whereas the Hsinhua fault, south of the CTFZ, is likely to mark the actual escape that prevails to the south.

6. Evidence of the onset of tectonic escape during the Quaternary from Quaternary stress patterns

An important point concerns the timing of the onset of the present-day tectonic escape inferred from GPS in SW Taiwan. Did this escape also occur (or begin) during the Quaternary?

In NE Taiwan, combined contractional, transcurrent, rotational and extensional tectonics in Quaternary formations provide evidence that escape tectonics was active during the Quaternary (Lu et al., 1995) (Fig. 1). In contrast, there is little direct structural evidence of Quaternary fault motion consistent with tectonic escape in SW Taiwan. A possible explanation could be that escape tectonics has a lower amplitude and began later in southern Taiwan than in northern Taiwan, in response to the obliquity of the collision and its subsequent southward migration.

Evidence for tectonic escape may nevertheless be brought by reconstruction of Quaternary paleostress patterns. A synthetic mapping of Quaternary $\sigma 1$ paleostress patterns in SW Taiwan is presented in Fig. 9 (detailed analysis of data collected in Quaternary formations not described herein, see for instance Lacombe et al., 1999). Two compressional stress regimes have regionally prevailed during the Quaternary: a NW–SE compression followed by a nearly E–W (WNW–ESE to ENE–WSW) compression. The first regime was clearly contractional and associated with the major stage of fold development, whereas the second regime generally prevailed during the latest stages of folding (at least south of the CTFZ) and was associated from north to south with an increasing component of perpendicular nearly N–S extension; the related structures evolving southward from strike-slip and reverse faults north of Tainan, to strike-slip and normal faults near Kaohsiung and to tension joints and normal faults to the south (Lacombe et al., 1999). These contrasting compressional trends, N120° and E–W on average, probably followed each other rapidly during the Pleistocene, and may reflect local changes of the kinematics of thrust units during this period.

Comparison between Quaternary and present-day stress and strain patterns allows discussion of whether the kinematics of structural units has recently changed or not in SW Taiwan. The nearly E–W contraction prevailed both during the late Quaternary and at present-day (Figs. 5 and 9B). Are the reconstructed paleostress patterns consistent with (and do they support) tectonic escape occurring (or beginning) during the late Quaternary? If so, is there any relation with the identified change in Quaternary stress regimes ? As mentioned previously, the absence of clear signature of the tectonic escape in the onland Quaternary deformation may be accounted for by a very recent beginning of this escape, which poorly influenced the already existing structural pattern. However, a possible signature of the onset of tectonic escape could be the change from the NW–SE to the nearly E–W (locally ENE–WSW, and even NE–SW: Fig. 9B) compression, the latter being consistent with (or maybe resulting from) an incipient right-lateral component of motion along NNE thrusts. Another possible signature could be the southward increasing occurrence of extensional features related to a nearly N–S extension during the latest stage of (or after) fold development (Lacombe et al., 1999). This along-strike change may indicate a southward decrease in N–S confinement during the late E–W shortening. This phenomenon is somewhat similar to (and consistent with) the present-day southward increase in extensional crustal strain relative to the regional N100° shortening deduced from GPS (Fig. 5): we propose that it supports a late Pleistocene onset of tectonic escape in SW Taiwan.

7. Offshore structural evidence for tectonic escape

Because escaping blocks and bounding discontinuities have been defined onland based on GPS and structural studies, it is important to find evidence that these discontinuities are extending offshore within the sedimentary wedge: it is also a test for our hypothesis of escape tectonics, which is expected to evolve southward as collision propagates.

Fig. 4 shows that the GPS station located on the Liukyu island (Liuc) displays a displacement velocity vector similar to that of the station S010 onshore. This suggests that according to our previous interpretation, both stations belong to the same rigid block (2), which can therefore be extended offshore (Fig. 6A).

Offshore structural evidence of escape tectonics are provided by swath bathymetric profiles and seismic lines which were recently acquired along WNW–

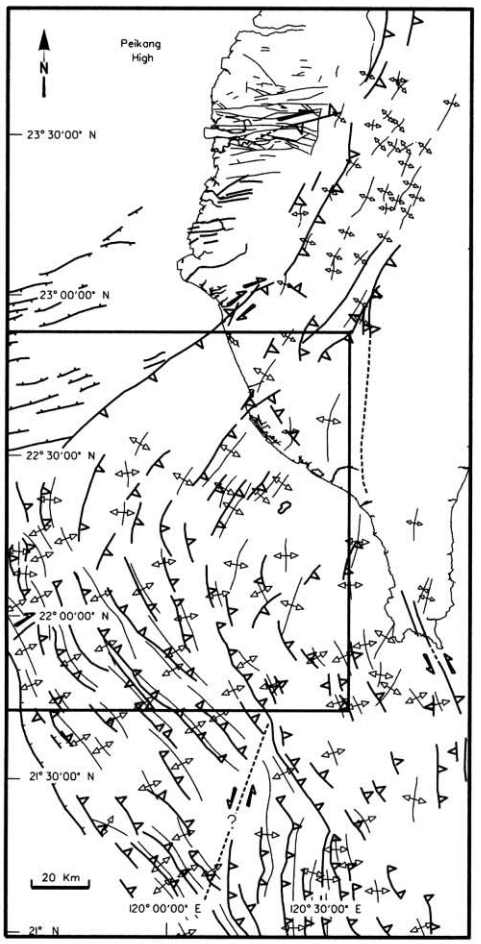
Peikang
High
N
23° 30'00" N
23° 00'00" N
22° 30'00" N
22° 00'00" N
21° 30'00" N
21° N
20 Km
120° 00'00" E
120° 30'00" E

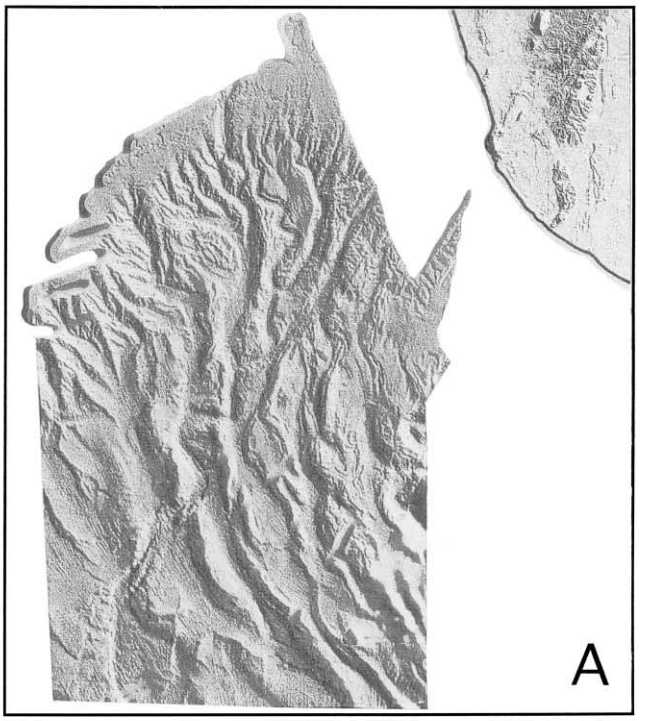
A

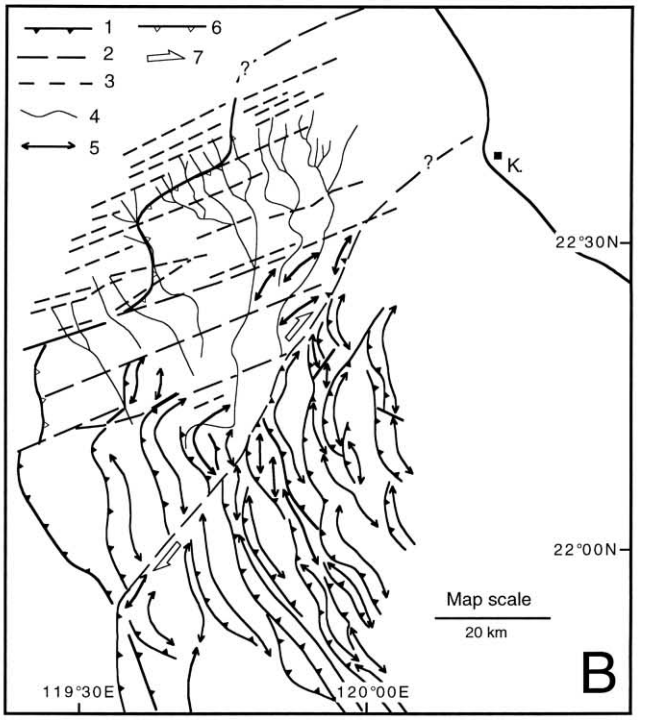
1
2
3
4
5
6
7
?
?
K.
22°30N
22°00N
Map scale
20 km
119°30E
120°00E
B

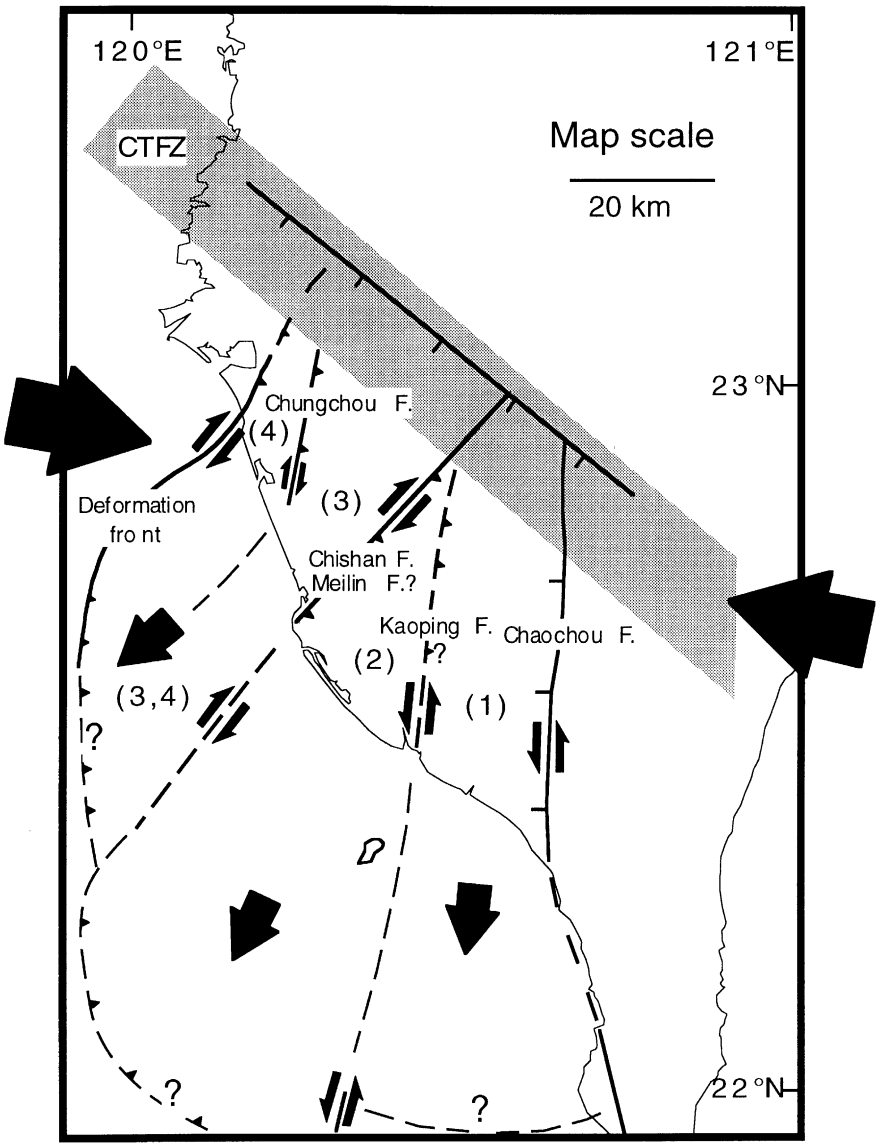

Fig. 11. Tentative model of escaping blocks in SW Taiwan. Arrows along the faults indicate the sense of along-strike component of motion. Note the inferred normal component of motion along the CTFZ.

Fig. 10. Structural offshore evidence for tectonic escape in SW Taiwan. Location map: modified and simplified after Deffontaines et al. (1999b). (A) Hill-shaded topographic–bathymetric map of SW Taiwan, vertical exaggeration ×2. Heavy line: shoreline. (B) Structural interpretation (Deffontaines et al., 1999a; this work): 1 — thrusts; 2 — inferred transverse faults within the wedge, along which bending of fold-thrust structures occur; 3 — inferred normal faults of the Chinese passive margin; 4 — rivers; 5 — anticline axis; 6 — inferred deformation front relocated based on combined analyses of bathymetry and unpublished seismic profiles; 7 — inferred right-lateral component of motion along the NE-trending transverse structure.

ESE and NNE–SSW trends during the Active Collision in Taiwan (ACT) cruise (May–June 1996). A preliminary structural interpretation of both the seismic lines and bathymetric maps has been briefly presented by Deffontaines et al. (1999a). Some of the main results, partly shown on the shaded bathymetric map of Fig. 10, are: (1) the general bend of fold-thrust structures from N020° to NE trends onland to N–S, and then to NNW–SSE trends in the southern part of the outer wedge (Reed et al. 1992); (2) the local ENE trend of frontal structures along the slope of the margin; and (3) the apparently lateral offset of folds against major normal faults (ENE trending) of the southern edge of the Peikang High. There is no evidence that these normal faults were reactivated as right-lateral compressional structures as in the NE part of the basin; however, their morphology has clearly locally guided the emplacement of the northernmost compressional structures of the prism. These results therefore confirm the location of the deformation front NW of Tainan (Fig. 10), which is consistent with earthquake occurrence offshore western Taiwan (Fig. 2).

The general bend of the outermost fold-thrust structures of the wedge, which locally follow the scarps of the ENE normal faults of the margin, in conjunction with some evidence of right-lateral motion along these locally ENE-trending structures (Fig. 1) support the tectonic escape toward the SW. An additional striking feature is the NE trending wrench structure within the wedge, well marked in the bathymetric morphology and exhibiting an apparent right-lateral component of motion (Fig. 10) (Deffontaines et al., 1999a). This inferred structure displays roughly the same trend as the Chishan/south Meilin fault system defined onland; it could represent, at least kinematically, its offshore southern extent. In the eastern part of the studied area (SW of the Hengchun peninsula), few clear structural features could be recognised from bathymetric analysis. A striking feature, nevertheless, consists of a NNE–SSW trending left-lateral strike-slip fault system (see location map of Fig. 10) inferred from several seismic sections across the frontal portion of the accretionary wedge (Fuh et al., 1997). The meandering course of the lower section of the Kaoping canyon (Liu et al., 1997) is very likely controlled by this fault system. Even though we have no structural information close to the coast, we propose that this left-lateral fault zone, which displays the same trend and is in the continuation of the onland inferred Kaoping fault zone, may belong to the same kinematic system.

In summary, the general bend of the outermost structures of the wedge along the Chinese margin as well as identification of wrench structures within the wedge, which could be linked to some active discontinuities limiting the blocks defined onland (Fig. 6D) support escape tectonics in SW Taiwan.

8. Tentative model of tectonic escape in SW Taiwan

Based on the above structural, geodetic and seismological evidence, we propose a new model of tectonic escape in SW Taiwan (Fig. 11).

The first point of this model is that tectonic escape is mainly restricted to the area south of the CTFZ, which appears as a major structural, seismological and kinematic boundary between a northern collision area undergoing active shortening and uplift (Chen, 1984) and a southern region which corresponds to the onland extension of the Manila accretionary wedge.

Second, the model assumes that escape tectonics is mainly limited to the 6 km thick cover, i.e. the sedimentary wedge (or maybe to the uppermost part of the crust). This relies upon the particular mechanical and kinematic behaviour of the SW Taiwan area south of the CTFZ. The earthquake distribution (Figs. 2 and 3) underlines the lack of shallow seismicity of this area, which additionally displays deviated GPS displacement velocity vectors with respect to the area north of the CTFZ. In contrast, the whole SW Taiwan Foothills show a pervasive N100–110° shortening at depth as indicated by earthquake focal mechanisms (Fig. 2C). This suggests that the SW Taiwan area limited by the deformation front and the Chaochou fault (Fig. 1) is strongly coupled at depth with the advancing units, whereas its sedimentary cover has a component of escape motion toward the SSW in addition to its nearly aseismic internal shortening. These particular mechanical behaviour and kinematics are restricted to the thick, fluid rich, poorly consolidated muddy cover, which is decoupled from

the deep basement above a 6 km-deep décollement which is expected to lie at the base of the neogene sedimentary pile. This décollement may correspond approximately to the base of the outer units of the Manila Accretionary wedge (Reed et al., 1992). This leads us to propose an offshore southward extension of the escaping area defined onland, its southern limit corresponding to the frontal thrusts of the wedge where the décollement merges (Fig. 11).

The third point is that the escaping area probably comprises four "rigid" (poorly internally deforming) blocks escaping at the present-day toward the SW along major discontinuities displaying a fan distribution and undergoing lateral slip in addition to reverse motion (Fig. 11).

Finally, this escape probably began during the late Pleistocene; this late onset, as well as the low amplitude compared to northern Taiwan, accounts for the few structural direct evidence of fault motion consistent with this escape.

9. Discussion and comparison with previous considerations on escape tectonics in SW Taiwan

Our model agrees with the results of Lu (1994) who proposed that escape tectonics was acting in SW (and NE) Taiwan, in response to the ongoing WNW convergence. Lu and Malavieille (1994) simulated the oblique collision of a deformable medium by an asymmetric rigid indentor, and showed that at the front of the indentor, pure contraction prevails, whereas stretching and wrenching accommodate the along-strike lateral extrusion of blocks moving toward the SW (and NE) tips of the belt. This suggests the occurrence of a tectonic escape in the broad sense, which is made possible by the low lateral confining conditions related to the Manila subduction zone to the south and the Ryukyu subduction zone — Okinawa Trough system to the north. Lateral extrusion has also been invoked in the Taiwan hinterland, this process accompanying the exhumation of the ductilely deformed metamorphic rocks of Central Range (Byrne et al., 1999).

More recent analogue modelling (Lu et al., 1998) suggests that the lateral escape of SW Taiwan is mainly influenced by the Peikang High, which acted as a local buttress for the advancing thrust units: this local indentor caused contraction against it and localised south of it a large dextral transfer zone around the shelf break of the Chinese continental margin, along which the SW Taiwan block was dragged to the SW; this general motion was made possible by a left-lateral motion along the N–S Chaochou shear zone (Biq, 1989).

Our results provide new evidence in favour of escape tectonics acting on the southern tip of the collision belt, toward the Manila subduction zone behaving as a free boundary. In this area, the process is probably enhanced by local indentation tectonics by the Peikang High (Lu et al., 1998). However, a significant difference between our's and Lu's (1994) model is that tectonic escape in SW Taiwan does not occur just along the southern edge of the Peikang High but rather south of the CTFZ, that is in the part of the Foothills which corresponds to the northern extent of the Manila accretionary wedge where actual collision is not yet active, probably in relation to the weak rheology of the wedge. Our model additionally considers several poorly internally deforming escaping blocks moving relative to each other; this hypothesis should be tested further. Finally, our model is in agreement with the numerical models of Hu et al. (1997) with the active velocity field and the tectonic stress pattern in SW Taiwan strongly depending on three factors: (1) the active frontal thrusts behaving as major "weak" discontinuities; (2) the presence and shape of the prominent Peikang basement high of the Chinese passive margin acting as a rigid indentor; and (3) the proximity of mechanical weakness zones corresponding to the Manila trench and the related accretionary prism.

Acknowledgements

The work was supported by the French Institute of Taipei — National Science Council of Taiwan cooperation framework, by the Central Geological Survey of Taiwan, and by the Institut Français du Pétrole. The authors would like to thank Prof. C.-S. Liu from National Taiwan University who kindly provided us with the hill-shaded bathymetric map of offshore SW Taiwan, and Dr Ruey-Juin Rau, Dr Desmond Darby, an anonymous referee and the Editor-in-Chief J.P. Burg for their constructive comments.

References

Angelier, J., 1990. Inversion of field data in fault tectonics to obtain the regional stress. III. A new rapid direct inversion method by analytical means. Geophys. J. Int. 103, 363–376.

Angelier, J., 1998. A new direct inversion of earthquake focal mechanisms to reconstruct the stress tensor, E.G.S. XXIII Gen. Assembly, Nice, 20–24 apr. 1998, Part I, Soc. Symp., Solid Earth Geoph. and Geod., Annales Geophysicae, vol. 16, suppl. 1, p. 115.

Angelier, J., Barrier, E., Chu, H.T., 1986. Plate collision and paleostress trajectories in a fold-thrust belt: the Foothills of Taiwan. Tectonophysics 125, 161–178.

Angelier, J., Chu, H.T., Lee, J.C., 1997. Shear concentration in a collision zone: kinematics of the Chihshang fault as revealed by outcrop-scale quantification of active faulting, Longitudinal Valley, eastern Taiwan. Tectonophysics 274, 117–143.

Angelier, J., Yu, S.B., Lee, J.C., Hu, J.C., Chu, H.T., 1999. Active deformation of Taiwan collision zone: discontinuities in GPS displacement field. Proceedings of the International symposium on Subduction et collision active dans le SE asiatique, Fourth colloquium on sino-french cooperation program in Earth sciences, Montpellier, France.

Barrier, E., Angelier, J., 1986. Active collision in eastern Taiwan: the Coastal Range. Tectonophysics 125, 39–72.

Biq, C., 1976. Western Taiwan earthquake-faults as miniature transform faults. Bull. Geol. Surv. Taiwan 25, 1–8.

Biq, C., 1989. The Yüshan–Hsüehshan megashear zone in Taiwan. Proc. Geol. Soc. China 32, 17–20.

Bonilla, M.G., 1975. A review of recently active faults in Taiwan. USGS Open-file report, 75-41, pp. 1–55.

Bonilla, M.G., 1977. Summary of Quaternary faulting and elevation changes in Taiwan. Mem. Geol. Soc. China 2, 43–56.

Byrne, T., Crespi, J., Pulver, M., Spiker, E., 1999. Deformation of the Taiwan hinterland: strike-slip faulting, extrusion or both? Proceedings of the International symposium on Subduction et collision active dans le SE asiatique, Fourth colloquium on sino-french cooperation program in Earth sciences, Montpellier, 9–12 May 1999.

Chen H., 1984. Crustal uplift and subsidence in Taiwan: an account based upon retriangulation results. Spec. Publ. Central Geol. Survey, 3, pp. 127–140 (in chinese).

Davis, D., Suppe, J., Dahlen, F.A., 1983. Mechanisms of fold-and-thrust belts and accretionary wedges. J. Geophys. Res. 88 (B2), 1153–1172.

Deffontaines, B., Lacombe, O., Angelier, J., Chu, H.-T., Mouthereau, F., Lee, C.-T., Deramond, J., Lee, J.-F., Yu, M.-S., Liew, P.-M., 1997. Quaternary transfer faulting in Taiwan Foothills: evidence from a multisource approach. Tectonophysics 274, 61–82.

Deffontaines, B., Liu, C.-S., Angelier, J., Mouthereau, F., Lacombe, O., 1999a. Quaternary tectonic evolution of offshore SW Taiwan. Proceedings of the International symposium on Subduction et collision active dans le SE asiatique, Fourth colloquium on sino-french cooperation program in Earth sciences, Montpellier, 9–12 May 1999.

Deffontaines, B., Chu, H.-T., Angelier, J., Lee, C.-T., Mouthereau, F., Li, F.-C., Brusset S., Chang, C.-P., Sibuet, J.-C., Chang, T.-Y., Lacombe, O., Liu, C.-S., Deramond, J., Lee, J.-C., Lu, C.-Y., Hu, J.-C., Yu, M.-S., Lee, J.-F., Bureau, D., 1999b Onshore–offshore Taiwan earth science data base within a geographical information system. Proceedings of the International symposium on Subduction et collision active dans le SE asiatique, Fourth colloquium on sino-french cooperation program in Earth sciences, Montpellier, 9–12 May 1999.

Fuh, S.-C., Liu, C.-S., Lundberg, N., Reed, D., 1997. Strike-slip faults offshore southern Taiwan: implications for the oblique arc–continent collision processes. Tectonophysics 274, 25–39.

Ho, C.S., 1986. A synthesis of the geologic evolution of Taiwan. Tectonophysics 125, 1–16.

Hu, J.C., Angelier, J., Yu, S.B., 1997. An interpretation of the active deformation of southern Taiwan based on numerical simulation and GPS studies. Tectonophysics 274 (1–3), 145–169.

Huang, C.-Y., Wu, W.-Y., Chang, C.-P., Tsao, S., Yuan, P.-B., Lin, C.-W., Kuan-Yuan, X., 1997. Tectonic evolution of accretionary prism in the arc–continent collision terrane of Taiwan. Tectonophysics 281, 31–51.

Hung, J.-H., Wiltschko, D.V., Lin, H.-C., Hickman, J.-B., Fang, P., Bock, Y., 1999. Structure and motion of the southwesern Taiwan fold-and-thrust belt. TAO 10 (3), 543–568.

Huiqi, L., McClay, K.R., Powell, D., 1992. Physical models of thrust wedges. In: Mc Clay, K.R. (Ed.). Thrust Tectonics. Chapman & Hall, London, pp. 71–81.

Hsu, T.-L., Chang, H.C., 1979. Quaternary faulting in Taiwan. Mem. Geol. Soc. China 3, 155–165.

Lacombe, O., Mouthereau, F., Deffontaines, B., Angelier, J., Chu, H.-T., Lee, C.T., 1999. Geometry and quaternary kinematics of fold-and-thrust units of SW Taiwan. Tectonics 18 (6), 1198–1223.

Lallemand, S.E., Tsien, H.-H., 1997. An introduction to active collision in Taiwan. Tectonophysics 274, 1–4.

Lallemand, S.E., Liu, C.-S., Font, Y., 1997. A tear fault boundary between the Taiwan orogen and the Ryukyu subduction zone. Tectonophysics 274 (1:3), 171–190.

Lee, T.Q., Angelier, J., 1995. Analysis of magnetic susceptibility anisotropy of the sedimentary sequences in southwestern foothills of Taiwan and its tectonic implications. Proceedings of the International conference and Third sino-french symposium on Active Collision in Taiwan, Abstracts volume, 22–23 March 1995, Taipei, Taiwan, pp. 213–218.

Le Pichon, X., Mazzotti, S., Henry, P., Hashimoto, M., 1998. Deformation of the Japanese Islands and seismic coupling: an interpretation based on GSI permanent GPS observations. Geophys. J. Int. 134, 501–514.

Liu, C.S., Huang, I.L., Teng, L.S., 1997. Structural features off southwestern Taiwan. Mar. Geol., 305–319.

Lu, C.Y., 1994. Neotectonics in the foreland thrust belt of Taiwan. Petrol. Geol. Taiwan 29, 15–35.

Lu, C.Y., Malavieille, J., 1994. Oblique convergence, indentation and rotation tectonics in the Taiwan Mountain belt: insights from experimental modelling. Earth Plan. Sci. Lett. 121, 477–494.

Lu, C.Y., Angelier, J., Chu, H.-T., Lee, J.-C., 1995. Contractional, transcurrent, rotational and extensional tectonics: examples from northern Taiwan. Tectonophysics 246, 129–146.

Lu, C.Y., Jeng, F.S., Chang, K.J., Jian, W.T., 1998. Impact of basement high on the structure and kinematics of the western Taiwan thrust wedge: insights from sandbox models. TAO 9 (3), 533–550.

Lundberg, N., Reed, D., Liu, C.-S., Lieske, J., 1997. Forearc-basin closure and arc accretion in the submarine suture zone south of Taiwan. Tectonophysics 274, 5–23.

Malavieille, J., 1999. Evolutionary model for arc–continent collision in Taiwan. Proceedings of the International symposium on Subduction et collision active dans le SE asiatique, Fourth colloquium on sino-french cooperation program in Earth sciences, Montpellier, 9–12 May 1999.

Mouthereau, F., Angelier, J., Deffontaines, B., Lacombe, O., Chu, H.T., Colletta, B., Déramond, J., Yu, M.S., Lee, J.F., 1996. Cinématique actuelle et récente du front de chaîne de Taiwan, C.R. Acad. Sci., t. 323, II, Paris, pp. 713–719.

Mouthereau, F., Angelier, J., Deffontaines, B., Brusset, S., Lacombe, O., Chu, H.-T., Déramond, J., 1998. Folds and fault kinematics and tectonic evolution of the southwestern thrust belt of onshore Taiwan. Annual meeting of Geological Society of China, Chungli, 20–21 March 1998, p. 140.

Mouthereau, F., Deffontaines, B., Lacombe, O., Angelier, J., 2001a. Along-strike variations of the Taiwan belt front: basement control on structural style, wedge geometry and kinematics. Geol. Soc. Am. Spec. Publ. (in press).

Mouthereau, F., Lacombe, O., Deffontaines, B., Angelier, J., Brusset, S., 2001b. Deformation history of the southwestern Taiwan foreland thrust belt: insights from tectono-sedimentary analysis and balanced cross-sections. Tectonophysics 333, 293–322.

Ratschbacher, L., Merle, O., 1991. Lateral extrusion in the Eastern Alps, part 2: structural analysis. Tectonics 2, 245–256.

Rau, R.J., Wu, F.T., 1998. Active tectonics of Taiwan orogeny from focal mechanisms of small-to-moderate earthquakes. TAO 9, 755–778.

Reed, D., Lundberg, N., Liu, C.-S., Kuo, B.-Y., 1992. Structural relations along the margins of the offshore Taiwan accretionary wedge: implications for accretion and crustal kinematics. Acta Geol. Taiwan. 30, 105–122 (Science reports of the National Taiwan University).

Rocher, M., Lacombe, O., Angelier, J., Chen, H.-W., 1996. Mechanical twin sets in calcite as markers of recent collisional events in a fold-and-thrust belt: evidence from the reefal limestones of southwestern Taiwan. Tectonics 15 (5), 984–996.

Sengör, A.M.C., Görür, N., Saroglu, F., 1985. Strike-slip faulting and related basin formation in zones of tectonic escape: Turkey as a case study. SEPM Spec. Publ. 37, 227–264.

Seno, T., Stein, S., Gripp, A.E., 1993. A model for the motion of Philippine Sea Plate consistent with NUVEL-1 and geological data. J. Geophys. Res. 98, 17 941–17 948.

Sun, S.C., Liu, C.S., 1993. Mud diapirs and submarine channel deposits in offshore Kaohsiung–Hengchun, southwest Taiwan. Petrol. Geol. Taiwan 28, 1–14.

Suppe, J., 1984. Kinematics of arc–continent collision, flipping of subduction, and back-arc spreading near Taiwan. Mem. Geol. Soc. China 4, 67–90.

Suppe, J., Hu, C.T., Chen, Y.-J., 1985. Present-day stress directions in western Taiwan inferred from borehole elongation. Petrol. Geol. Taiwan 21, 1–12.

Tapponnier, P., Peltzer, A., Le Dain, Y., Armijo, R., Cobbold, P., 1983. Propagating extrusion tectonics in Asia: new insights from simple experiments with plasticine. Geology 10, 611–616.

Teng, L.S., 1990. Geotectonic evolution of late Cenozoic arc–continent collision in Taiwan. Tectonophysics 183, 57–76.

Tsai, Y.-B., 1986. Seismotectonics of Taiwan. Tectonophysics 125, 17–37.

Wu, F., Rau, R.-J., Salzberg, D., 1997. Taiwan orogeny: thin-skinned or lithospheric collision?. Tectonophysics 274, 191–200.

Yeh, Y.H., Barrier, E., Angelier, J., 1991. Stress tensor analysis in the Taiwan area from focal mechanisms of earthquakes. Tectonophysics 200, 267–280.

Yu, S.B., Chen, H.Y., 1996. Spatial variation of crustal strain in the Taiwan area, Sixth Taiwanese Geophysical Meeting, Chiayi, November 1996, abstract volume, pp. 659–668.

Yu, S.B., Chen, H.Y., 1998. Strain accumulation is Southwestern Taiwan. TAO 9 (1), 31–50.

Yu, S.-B., Chen, H.-Y., Kuo, L.-C., 1997. Velocity field of GPS stations in the Taiwan area. Tectonophysics 274, 41–59.

Yu, S.-B., Kuo, L.-C., Punongbayan, R.S., Ramos, E.G., 1999. GPS observation of crustal deformation in the Taiwan–Luzon region. Geophys. Res. Lett. 26 (7), 923–926.